Macromolecules

ARTICLE

pubs.acs.org/Macromolecules

Relaxation of Single Polymer Chain in Poly(methyl methacrylate) Films under Uniaxial Extension Observed by Scanning Near-Field Optical Microscopy

Toru Ube,[†] Hiroyuki Aoki,[*,†,‡] Shinzaburo Ito,[†,‡] Jun-ichi Horinaka,[§] Toshikazu Takigawa,[§] and Toshiro Masuda[§]

[†]Department of Polymer Chemistry, Graduate School of Engineering, Kyoto University, Nishikyo, Kyoto 615-8510, Japan

[‡]Advanced Biomedical Engineering Research Unit, Kyoto University, Nishikyo, Kyoto 615-8510, Japan

[§]Department of Material Chemistry, Graduate School of Engineering, Kyoto University, Nishikyo, Kyoto 615-8510, Japan

ABSTRACT: Single chain conformations during the stress relaxation process in uniaxially stretched poly(methyl methacrylate) (PMMA) films were observed in real space by scanning near-field optical microscopy (SNOM). The extension ratio at the molecular level was directly evaluated from the SNOM images and compared with the macroscopic stress relaxation. At the early stage of the relaxation process, the whole single chain retained the stretched conformation in spite of the decrease in stress. This suggests that the fast relaxation in stress is caused by the local conformational change at the length scale much smaller than the entire chain length. The experimental data were successfully explained by the contraction of the primitive chain contour in the Doi−Edwards model. Furthermore, the distribution function of the chain dimension was found to retain its shape during the relaxation process, indicating that the conformational relaxation of polymer chain is rather homogeneous in the well-entangled system.

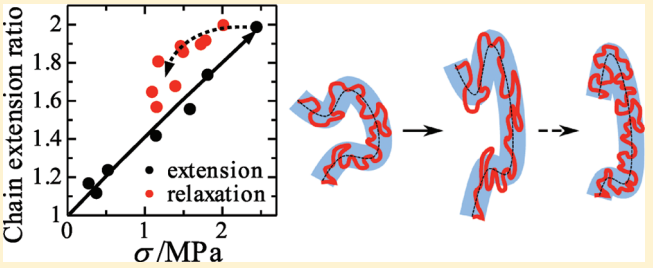

1. INTRODUCTION

The relaxation behavior of polymer melts has long been investigated because of its importance both in scientific and industrial fields. The stress induced by an external strain is relaxed through the motion of deformed polymer chains to the equilibrium conformations. In entangled polymer systems, the relaxation is slow because of the mutual uncrossability of the chains. The dynamics in such systems has been explained by the molecular models based on the tube model by de Gennes[1] and Doi and Edwards .[2−5] In the Doi−Edwards model, the chain motion is constrained in a tubelike region surrounding the chain backbone. When the system is deformed by a step strain, the chain changes in conformation according to affine deformation. Then, these chains relax through the motions along the tube: the contraction of the chain contour and the reptation. The stress is calculated under these assumptions of the chain dynamics. The tube model has been improved to explain the viscoelastic properties of various systems by considering the contour length fluctuation and the relaxation of surrounding chains.[6,7] While theoretical molecular models express the mechanical properties and have been compared with rheological experiments, they also predict the time evolution of the chain conformation. The observations of the polymer chain at the various length scales are essential to evaluate the chain motion, which is assumed in theoretical models. The average dimension of a whole single chain under the external force has been measured by small-angle neutron scattering (SANS) in concentrated polymer systems.[8−12] The recent improvement of the SANS instrument enabled the detection of the conformational relaxation consistent with the contraction of the chain contour.[12] The scattering measurement has great advantage in the high resolution, but the variety of chain conformations is canceled in the value averaged over the bulk sample. The observation of individual single polymer chains could reveal the exact behavior of real chains, which possibly depends on initial chain conformations and surrounding conditions. The understanding of the distribution of the chain motion will lead to the improvement of theoretical models, which have been based on the preaveraged chain dynamics.[7]

In order to detect in-situ features of polymer chains inside a bulk medium, we must distinguish a single chain from its surroundings. Fluorescence labeling is an established method, which has been applied to observe single DNA molecules. Perkins et al. succeeded in the direct observation of the tubelike motion of DNA chains by fluorescence microscopy.[13] The conformational changes of DNA molecules in a dilute and entangled solution under flow have also been studied.[14,15] However, conventional fluorescence microscopy has a low spatial resolution of ∼250 nm due to the diffraction limit of light.

Received: March 4, 2011
Revised: April 22, 2011
Published: May 10, 2011

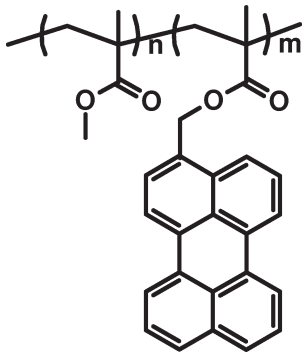

Figure 1. Chemical structure of random copolymer PMMA-Pe.

Table 1. Characterization of PMMA

sample	$M_w/10^6$	$M_n/10^6$	M_w/M_n
PMMA-Pe	1.99	1.58	1.26
PMMA	1.89	1.53	1.24

Therefore, the application of optical microscopy to single macromolecular imaging has been limited to the observation of huge biomacromolecules such as DNA. Scanning near-field optical microscopy (SNOM) is an emerging scanning probe technique which allows optical measurement with a high resolution beyond the diffraction limit.[16,17] The light incidence to a subwavelength-sized aperture generates an optical near-field restricted in the space of the aperture size. This allows one to illuminate a specimen and to obtain the optical response from the nanometric area. Therefore, SNOM enables us to directly observe the conformation of the single chain, which is fluorescently labeled and silhouetted against surrounding unlabeled polymers.[18−22]

Our previous study on poly(methyl methacrylate) (PMMA) chains in the films under uniaxial deformation revealed that the dimension of the whole single chain increased affinely with the macroscopic strain when the film is stretched well above the glass transition temperature.[22] Here we examined the chain conformation during the stress relaxation process by SNOM in contrast with the stress and the birefringence. We compared the experimental results with the theoretical prediction by the Doi−Edwards model.

2. EXPERIMENTS

Sample Preparation. Perylene-labeled PMMA (PMMA-Pe, Figure 1) was synthesized by random copolymerization of methyl methacrylate and 3-perylenylmethyl methacrylate as described elsewhere.[21,23] The fraction of the labeled unit was evaluated to be 0.77% by UV−vis absorption (U3500, Hitachi). The unlabeled PMMA was synthesized by atom transfer radical polymerization.[24] Methyl methacrylate was polymerized with *p*-toluenesulfonyl chloride in conjunction with copper(I) chloride and 4,4′-dinonyl-2,2′-dipyridyl at 70 °C in vacuum. The weight- and number-averaged molecular weights, M_w and M_n, were determined by GPC measurement as shown in Table 1.

In order to observe single labeled chains in the PMMA bulk by SNOM, we prepared the sample containing a trace amount of PMMA-Pe near the surface by the following procedure. A mixed toluene solution of unlabeled PMMA and PMMA-Pe (0.005 wt % to the unlabeled polymer) was spin-coated onto a glass substrate to form an 80 nm thick film. The thin film was floated on water and deposited on a self-standing thick film of unlabeled PMMA (the size was 25 mm × 7 mm and the thickness was 300 μm), which was prepared separately by the solution casting. The conformation of PMMA-Pe may be affected by the shear flow in the spin-coating process and the confinement effect of the thin film. Therefore, the sample film was annealed for 48 h at 200 °C, which is longer than the relaxation time estimated from the literature,[25] in vacuum to reach the equilibrium.

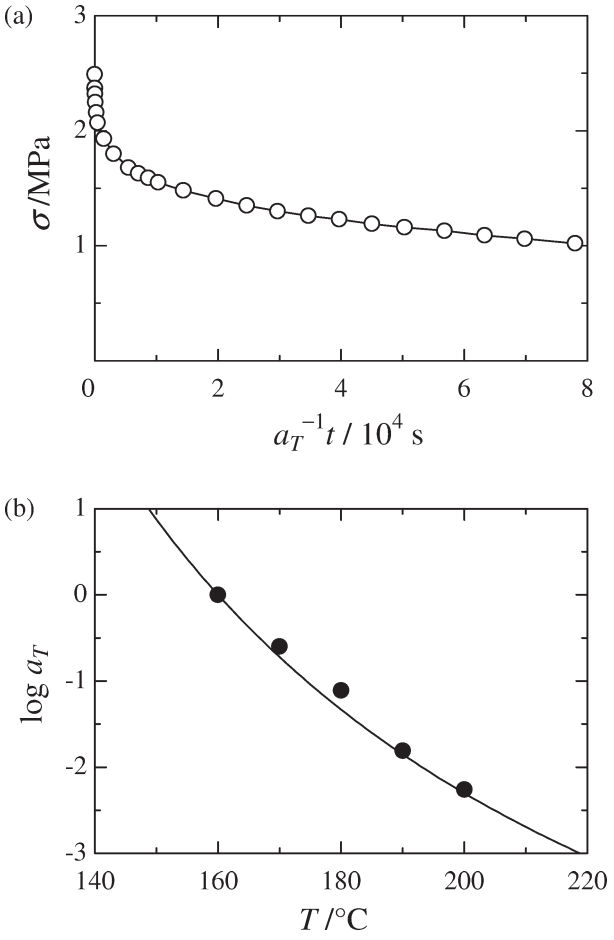

Figure 2. (a) Stress relaxation master curve for the PMMA film with λ = 2.0 at 160 °C. (b) Shift factor of PMMA to form the master curve. The solid curve represents the WLF equation (eq 2).

Tensile Deformation. A tensile tester (RTM-500, Orientec) with a 10 kg load cell was used for stretching the films. The length between the clamps was 20 mm. The stretching was carried out at 160−200 °C with a crosshead speed of 50 mm/min. After the stretching, the clamp gap was kept constant for time *t*. Then the films were immediately quenched to room temperature. The force was monitored on a chart recorder throughout the stretching and relaxation processes. The extension ratio, λ, was calculated as l/l_0 where l_0 and l are the lengths of the film along the stretching direction before and after the elongation, respectively. The true stress, σ, was evaluated as follows assuming the constant volume of the film:

$$\sigma = \frac{F}{A} = \frac{F}{A_0}\lambda \quad (1)$$

where F is the force applied to the sample, A is the sample cross section at the extension ratio of λ, and A_0 is the cross section at $\lambda = 1$.

Birefringence Measurement. The birefringence measurement was carried out by the Senarmont method. The optical system was composed of a laser, a polarizer, a quarter-wave plate, an analyzer, and a photodetector. The axes of the polarizer and the quarter-wave plate were set at 45° to the strain axis. After passing through the oriented sample, the

dx.doi.org/10.1021/ma2004986 |*Macromolecules* 2011, 44, 4445–4451

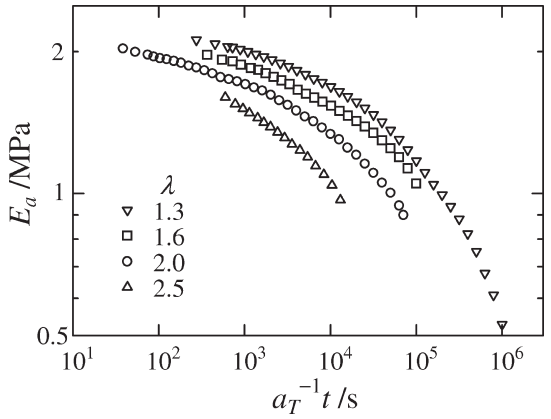

Figure 3. Apparent Young's modulus plotted against time, which was reduced to 160 °C.

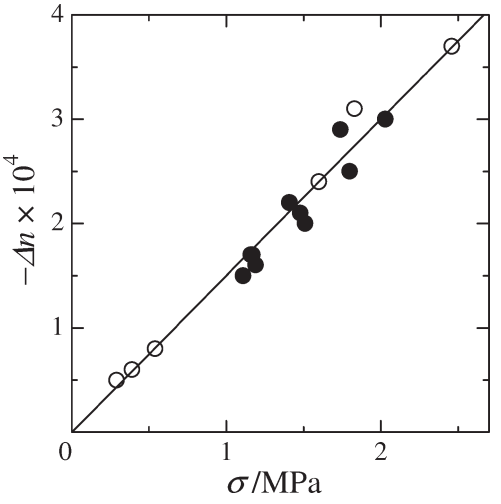

Figure 4. Birefringence plotted against stress. Open and closed circles represent the extension and relaxation processes, respectively.

plane-polarized light becomes elliptically polarized. The quarter-wave plate converts it into linearly polarized light, the direction of which is different from the initial polarization by an angle φ. The retardation, Γ, was evaluated as $\Gamma = \lambda_L(\varphi/\pi)$, where λ_L is the incident wavelength. The accuracy of Γ in this measurement was better than 3 nm. The birefringence, Δn, was determined as $\Delta n = \Gamma/d$, where d is the sample thickness.

SNOM Measurement. The SNOM measurement was performed by a commercially available instrument (α-SNOM, WITec) using a hollow cantilever probe with a subwavelength aperture of 60 nm. The laser beam at a wavelength of 438 nm (BCL-015-440, CrystaLaser) was focused onto the backside of the aperture to generate the optical near-field. While scanning the sample surface in the contact mode with the cantilever, the perylene fluorescence was collected by a microscope objective (0.80 NA, 60×, Nikon) from the backside of the substrate, passed through a long-pass filter (AELP454, Omega Optical), and detected with a photomultiplier (H8631, Hamamatsu Photonics). The SNOM measurement was carried out in an ambient condition. All the SNOM images were taken by the same probe.

3. RESULTS AND DISCUSSION

Figure 2a shows a stress relaxation curve of the PMMA film after the tensile deformation of $\lambda = 2.0$. We applied the time−temperature superposition principle to obtain the master curve at a reference temperature $T_r = 160$ °C. The stress monotonously decreased with time. The shift factor, a_T, used to obtain the master curve is shown in Figure 2b. The solid curve in Figure 2b represents the WLF equation

$$\log a_T = -\frac{9.78(T - T_r)}{130 + T - T_r} \quad (2)$$

which is consistent with the literature.[25]

The strain dependence of the stress relaxation was investigated in terms of the apparent Young's modulus defined by $E_a = 3\sigma/(\lambda^2 - \lambda^{-1})$.[26] Figure 3 shows E_a of the PMMA films stretched to $\lambda = 1.3-2.5$ plotted against time. If the strain is within the linear regime, E_a would be independent of strain. In the time range of this experiment, E_a depended on the strain and the curves were not parallel: the larger the strain was, the faster E_a decreased. This fast relaxation is attributed to the contraction presented in the Doi−Edwards theory. In the rest of this paper, the case of $\lambda = 2.0$ is investigated.

Figure 4 shows the birefringence plotted against the stress, in which the data for the extension process (open circles) from our previous paper[22] are also shown. The birefringence was in proportion to the stress in both the extension and relaxation processes according to the stress−optical rule[5]

$$\Delta n = C\sigma \quad (3)$$

where C is the stress−optical coefficient. The value of C was evaluated to be -1.5×10^{-10} Pa^{-1}, which is in good agreement with the values reported in the literature .[27,28] Since the birefringence arises from the orientational anisotropy of the monomers, the stress is directly related to the orientation of the chain backbone.

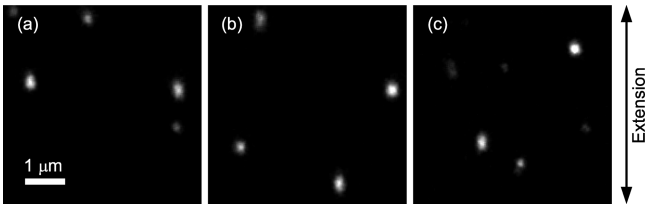

Figure 5. Fluorescence SNOM images of single polymer chains in the PMMA films, which were quenched immediately after the stretching (a) and after the relaxation periods, $a_T^{-1}t$, of 3.6×10^3 s (b) and 7.1×10^4 s (c). The macroscopic extension ratio is 2.0.

Figure 5 shows the fluorescence SNOM images of the PMMA films immediately after stretching (a) and during the stress relaxation process (b, c). The perylene-labeled PMMA chains embedded in the unlabeled bulk film were observed as bright spots in the fluorescence image. Each fluorescence spot was confirmed to be individual PMMA-Pe chain from the statistical analysis.[21] Since the optical near-field penetrates into the sample film by a few hundred nanometers, the shape of the PMMA chain observed in the SNOM image is given as a two-dimensional projection of the chain conformation. These images clearly show the polymer chains with elongated conformations along the macroscopic stretching direction. The stresses of the samples in panels a, b, and c of Figure 5 were 2.46, 1.74, and 1.17 MPa, respectively. Even during this stress relaxation process, many of the chains showed elongated conformations as shown in panels b and c of Figure 5.

The conformation of the single PMMA chain was quantitatively evaluated from the fluorescence intensity distribution.[20] The fluorescence intensity is proportional to the number of

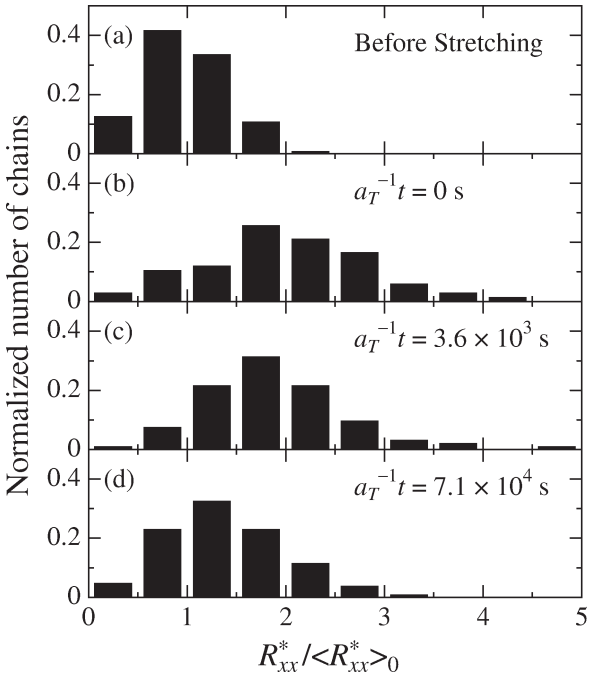

Figure 6. Histograms of the chain dimension parallel to the stretching direction, which was normalized by the initial average value, in the films before stretching (a), quenched immediately after the stretching (b), and after the relaxation periods, $a_T^{-1}t$, of 3.6×10^3 s (c) and 7.1×10^4 s (d).

fluorescence dye molecules randomly introduced to the PMMA-Pe chain; therefore, the intensity at each pixel is proportional to the number of the chain segment therein. We selected an area including a single chain in the fluorescence image and read the fluorescence intensity at each pixel throughout this area. The first moment of the fluorescence intensity distribution denotes the position of the center of mass

$$\mathbf{r}_0 = \frac{1}{I}\sum_i \mathbf{r}_i I_i \tag{4}$$

where I_i is the fluorescence intensity at the ith pixel, $\mathbf{r}_i$ is the position vector, and I is the total fluorescence intensity from the single chain. The second moment of the fluorescence intensity distribution along the x axis is calculated as

$$R_{xx}{}^2 = \frac{1}{I}\sum_i (x_i - x_0)^2 I_i \tag{5}$$

where x_i and x_0 are the x-coordinate of the ith pixel and the center of mass, respectively. We define the x axis as the macroscopic extension axis of the film. R_{xx} indicates the dimension of the fluorescence spot along the x axis. SNOM shows much higher resolution than conventional microscopy, but it still suffers from the limit of finite resolution of ~100 nm, which is caused by finite dimension of the aperture. Therefore, the observed value of R_{xx} is somewhat larger than the true dimension of the chain, $R_{xx}{}^*$, which is defined by

$$R^*_{xx}{}^2 = \frac{1}{N}\sum_j^N (x_j - x_0)^2 \tag{6}$$

where N is the number of segments and x_j is the x-coordinate of the position of the jth segment of the chain.[29] The point spread function in the fluorescence SNOM measurement is well approximated as a Gauss function, which was determined from the observation of a quantum dot.[20] The fluorescence image is expressed by the convolution of the spatial distribution of the chain segment and the point spread function. The second moment of the convoluted function is a sum of the second moments of the original functions. Therefore

$$R_{xx}{}^2 = R^*_{xx}{}^2 + a^2 \tag{7}$$

where a^2 is the variance of the point spread function. R^*_{xx} reflects the dimension of the whole single chain along the extension axis. As for the direction perpendicular to the stretching axis, the change in the dimension was too small for the precise evaluation. Therefore, we focused on the direction parallel to the stretching axis.

The results of the statistical analysis for 100−150 chains are summarized in Figure 6, which shows histograms for the dimension of the chain along the stretching direction normalized by the initial average, $\langle R^*_{xx}\rangle_0$. Figure 6a shows the conformational distribution of flexible PMMA chains in the equilibrium state. The dimension of each chain increased by the stretching of the film (Figure 6b). The distribution of $R^*_{xx}/\langle R^*_{xx}\rangle_0$ did not significantly change at the early stage of the relaxation process (Figure 6c). The chain dimension clearly decreased for the samples with a longer relaxation period (Figure 6d).

We first focus on the time evolution of the average value in terms of the molecular extension ratio at the single chain level, λ_c, which we define as

$$\lambda_c{}^2 = \frac{\langle R^*_{xx}{}^2\rangle}{\langle R^*_{xx}{}^2\rangle_0} \tag{8}$$

where $\langle R^*_{xx}{}^2\rangle_0$ and $\langle R^*_{xx}{}^2\rangle$ denote the square average of the true dimension of the chains along the x axis before and after stretching. Figure 7 shows λ_c and the stress plotted against time. Soon after the stretching, λ_c was equal to the macroscopic extension ratio of the film, λ, showing the affine deformation.[22] The macroscopic stress decreased over the whole time range of the observation. On the other hand, λ_c almost kept the initial value of 2.0 at the early stage of the stress relaxation process

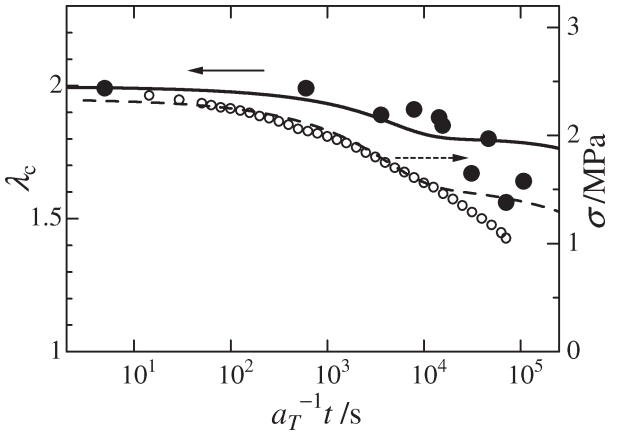

Figure 7. Chain extension ratio (closed circles) and stress (open circles) plotted against time, which was reduced to 160 °C. The macroscopic extension ratio is 2.0. Solid and dashed curves indicate the chain extension ratio and the stress calculated from the Doi−Edwards model, respectively.

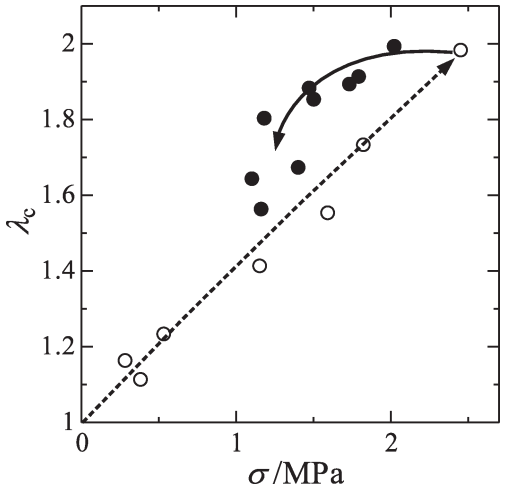

Figure 8. Chain extension ratio plotted against stress. Open and closed circles represent the extension and relaxation processes, respectively.

($a_T^{-1}t < 1 \times 10^4$ s). This indicates that the whole chain kept a stretched conformation in the short time scale in spite of the decrease in the stress.

Figure 8 shows λ_c plotted against the stress during the extension (data from our previous paper[22]) and relaxation processes. In the extension process, λ_c increased with the stress. At the early stage of the relaxation process, however, the extension ratio of the single chain was not dependent on the decrease in the stress. λ_c does not directly correspond with the stress, whereas the birefringence is related to the stress (Figure 4).

We compared the experimental data with the Doi−Edwards model. First, the affine deformation is assumed for a step strain. The contour length, L, and the orientation of the primitive chain are increased by the deformation. Then, the relaxation takes place through following three steps: (A) the redistribution of monomers between the entanglements, (B) the contraction of the chain contour, and (C) the reptation of the entire chain with the relaxation times of τ_A, τ_B, and τ_C, respectively. In step A, the stress decreases according to $\sigma \propto t^{-1/2}$. In the time scale of the current experiment, this fast relaxation was not observed. Since step A does not affect the conformation of the whole chain, $\langle R_{xx}^{*\,2}\rangle$ and $\langle L\rangle$ are the same with those after the affine deformation: $\langle R_{xx}^{*\,2}\rangle = \lambda^2\langle R_{xx}^{*\,2}\rangle_0$ and $\langle L\rangle = \alpha\langle L_0\rangle$, where α is the average stretch ratio of the contour length of the primitive chain and L_0 is L at the equilibrium. α is a monotonically increasing function with strain: $\alpha = 1.23$ for the uniaxial extension of $\lambda = 2.0$.[5] At step B, where L reduces to L_0, the stress decreases by a factor of $1/\alpha^2$ through the decrease in the contour length and the increase in the number of monomers between entanglements. When the Rouse model is applied to step B, the time evolution of $\langle L\rangle$ is given by $\langle L\rangle = \langle L_0\rangle\mu_B$,[4,5] where

$$\mu_B = \sum_{p=1,3,5,\ldots}^{\infty} \frac{8}{p^2\pi^2}\left\{1 + (\alpha - 1)\exp\left(-\frac{tp^2}{\tau_B}\right)\right\} \quad (9)$$

Under this assumption, the stress is expressed as

$$\sigma = \frac{15}{4} G_N^0 Q\mu_B{}^2 \quad (10)$$

where G_N^0 is plateau modulus and Q denotes the orientation immediately after the step strain ($Q = 0.580$ for $\lambda = 2$).[5] On the other hand, $\langle R_{xx}^{*\,2}\rangle$ decreases by a factor of $1/\alpha$ in proportion to $\langle L\rangle$:[3,30]

$$\langle R_{xx}^{*\,2}\rangle = \langle R_{xx}^{*\,2}\rangle_0 \frac{\lambda^2}{\alpha}\mu_B \quad (11)$$

The relaxation time of step B is $\tau_B = 2\tau_A(M/M_e)^2$, where M_e is the molecular weight between entanglements: $M_e = \rho RT/G_N^0$, where ρ is the density, R is the gas constant, and T is the temperature. At step C, the conformation is relaxed to the equilibrium through reptation. The stress and $\langle R_{xx}^{*\,2}\rangle$ are related to the fraction of the primitive chain segment in the original tube:[2,4,30]

$$\sigma = \frac{15}{4} G_N^0 Q\mu_B{}^2\mu_{C1} \quad (12)$$

$$\langle R_{xx}^{*\,2}\rangle = \langle R_{xx}^{*\,2}\rangle_0\left\{\left(\frac{\lambda^2}{\alpha}\mu_B - 1\right)\mu_{C2} + 1\right\} \quad (13)$$

where

$$\mu_{C1} = \sum_{p=1,3,5,\ldots}^{\infty} \frac{8}{p^2\pi^2}\exp\left(-\frac{tp^2}{\tau_C}\right) \quad (14)$$

$$\mu_{C2} = \sum_{p=1,3,5,\ldots}^{\infty} \frac{96}{p^4\pi^4}\exp\left(-\frac{tp^2}{\tau_C}\right) \quad (15)$$

From eq 13

$$\lambda_c = \left\{\left(\frac{\lambda^2}{\alpha}\mu_B - 1\right)\mu_{C2} + 1\right\}^{1/2} \quad (16)$$

The relaxation time of step C is $\tau_C = 6\tau_A(M/M_e)^3$.

We fitted the stress relaxation curve using eq 12 with τ_A and the plateau modulus G_N^0 as the fitting parameters. The theoretical stress relaxation curve is shown as a dashed curve in Figure 7. The best fit values were $\tau_A = 2.0 \times 10^{-2}$ s and $G_N^0 = 0.72$ MPa. Although the plateau modulus of PMMA strongly depends on the tacticity,[31] these values are within the range of the experimental values obtained from shear measurements in the literature.[26,31] The relaxation times of steps B and C were calculated as $\tau_B = 4.5 \times 10^3$ s and $\tau_C = 4.5 \times 10^6$ s, respectively. Therefore, the stress relaxation is mainly caused by step B in the time range of this experiment. This is consistent with the strain-dependent decrease of the relaxation modulus shown in Figure 3 because step B is a strain-dependent process. The inconsistency between the experimental and theoretical values at the longer time ($a_T^{-1}t > 1 \times 10^4$ s) may be caused by the motion of the matrix chains, which leads to disentanglement. Using the parameters obtained from the analysis of the stress relaxation, we calculated the theoretical curve for λ_c from eq 16 (solid curve in Figure 7). The theoretical prediction was consistent with the experimental data in the time range of $a_T^{-1}t < 1 \times 10^4$ s, showing the slow reduction of λ_c. At step B, the reduction of λ_c originates from the decrease in contour length. On the other hand, the stress reduces through not only the decrease in contour length but also the increase in the number of monomers between entanglements. The faster relaxation in stress is caused by the conformational change at the small length scale, which hardly affects the dimension of the whole chain level.

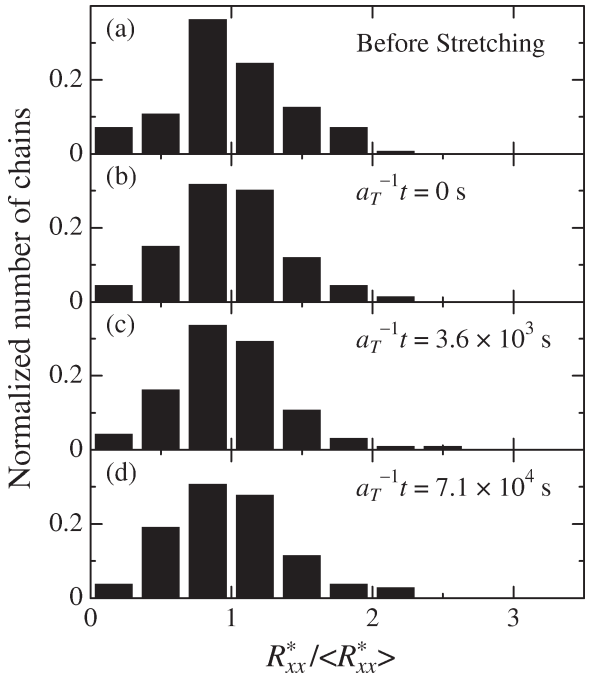

Figure 9. Histograms of the chain dimension parallel to the stretching direction, which was normalized by the average value for each sample, in the films before stretching (a), quenched immediately after the stretching (b), and after the relaxation periods, $a_T^{-1}t$, of 3.6×10^3 s (c) and 7.1×10^4 s (d).

We should consider the fact that the labeled polymer chains exist near the surface in our system. The chain behavior near the surface would be different from that of the bulk because of the lowered entanglement density near the surface.[32] This would accelerate the relaxation of labeled polymer chains at the whole chain level. However, the experimental result shows that the relaxation of the whole chain is still slower than that of the bulk stress. It seems that the surface effect is not large enough to affect the values of λ_c in the condition of the current experiment.

The ensemble-averaged chain dimension can be analyzed also from SANS measurements. The previous SANS studies on entangled polystyrene melts under flow showed that the birefringence relaxed faster than the orientation at the length scale of the entire chain.[10,11] The result obtained from the direct observation of the individual polymer chains by SNOM was consistent with the SANS studies, indicating the significance of the contraction process in the nonlinear region.

We next focus on the distribution function of R^*_{xx}. In the contraction process, the degree of relaxation could be different for each chain because the stretch ratio of the chain contour, L/L_0, could be different for each chain: the chain with a larger L/L_0 shows a larger relaxation through the contraction.[7] This leads to a change in the shape of the distribution function for R^*_{xx}. In order to focus on the shape of the distribution function, the histograms of R^*_{xx} in Figure 6 were redrawn to Figure 9 in terms of the chain dimension normalized by the average value of each sample, $R^*_{xx}/\langle R^*_{xx}\rangle$. In the film immediately after stretching (panel b in Figure 9), the shape of the distribution function of $R^*_{xx}/\langle R^*_{xx}\rangle$ did not significantly change from that before stretching (panel a). This is consistent with the picture of the affine deformation. Every chains are stretched with a given molecular extension ratio λ_c, which is equal to the macroscopic extension ratio. In the stress relaxation process (panels c and d), the distribution functions retained the shape. This implies that each chain has a similar stretch ratio of the chain contour L/L_0 and also shows similar relaxation behavior in the contraction process. This is probably due to the high molecular weight of the sample. In the present case, the number of entanglement segments per chain was large: $M_w/M_e \approx 340$. Therefore, the orientation of the primitive chain segment was well averaged over the whole single chain. This intramolecular statistics leads to the similar L/L_0 values of every chain and consequently the homogeneous relaxation during the contraction process.

4. CONCLUSION

The relaxation of single PMMA chains in a uniaxially stretched film was directly observed by SNOM in real space. We found that the whole chain kept an elongated conformation in spite of the decrease in stress at the early stage of the relaxation process. The experimental data were consistent with the contraction process in the Doi−Edwards model. This suggests that the faster relaxation in stress is caused by the conformational change at the small length scale, which hardly affects the conformation at the whole chain scale. The shape of the distribution function of the chain dimension did not change significantly during the relaxation process, implying homogeneous chain relaxation on a whole chain scale for the well-entangled system. Thus, direct observation of the single chain enables us to investigate the polymer physics considering the individual behaviors of polymer chains.

AUTHOR INFORMATION

Corresponding Author

*E-mail: aoki@photo.polym.kyoto-u.ac.jp.

ACKNOWLEDGMENT

This work is supported by Grants-in-Aid from Ministry of Education, Culture, Sports, Science and Technology, Japan (MEXT). The authors acknowledge also the Innovative Techno-Hub for Integrated Medical Bioimaging Project of the Special Coordination Funds for Promoting Science and Technology from MEXT. T.U. thanks Research Fellowships of the Japan Society for the Promotion of Science for Young Scientists.

REFERENCES

(1) de Gennes, P. G. *J. Chem. Phys.* **1971**, *55*, 572–0.
(2) Doi, M.; Edwards, S. F. *J. Chem. Soc., Faraday Trans. 2* **1978**, *74*, 1789–1801.
(3) Doi, M.; Edwards, S. F. *J. Chem. Soc., Faraday Trans. 2* **1978**, *74*, 1802–1817.
(4) Doi, M. *J. Polym. Sci., Polym. Phys. Ed.* **1980**, *18*, 1005–1020.
(5) Doi, M.; Edwards, S. F. *The Theory of Polymer Dynamics*, 3rd ed.; Clarendon: Oxford, 1986.
(6) Watanabe, H. *Prog. Polym. Sci.* **1999**, *24*, 1253–1403.
(7) McLeish, T. C. B. *Adv. Phys.* **2002**, *51*, 1379–1527.
(8) Boué, F.; Nierlich, M.; Jannink, G.; Ball, R. *J. Phys. (Paris)* **1982**, *43*, 137–148.
(9) Boué, F. *Adv. Polym. Sci.* **1987**, *82*, 47–101.
(10) Bent, J.; Hutchings, L.; Richards, R. W.; Gough, T.; Spares, R.; Coates, P. D.; Grillo, I.; Marien, O. G.; Read, D. J.; Graham, R. S.; Likhtman, A. E.; Groves, D. J.; Nicholson, T. M.; McLeish, T. C. B. *Science* **2003**, *301*, 1691–1695.

(11) Graham, R. S.; Bent, J.; Hutchings, L. R.; Richards, R. W.; Groves, D. J.; Embery, J.; Nicholson, T. M.; McLeish, T. C. B.; Likhtman, A. E.; Harlen, O. G.; Read, D. J.; Gough, T.; Spares, R.; Coates, P. D.; Grillo, I. *Macromolecules* **2006**, *39*, 2700–2709.
(12) Blanchard, A.; Graham, R.; Heinrich, M.; Pyckhout-Hintzen, W.; Richter, D.; Likhtman, A.; McLeish, T.; Read, D.; Straube, E.; Kohlbrecher, J. *Phys. Rev. Lett.* **2005**, *95*, 166001.
(13) Perkins, T. T.; Smith, D. E.; Chu, S. *Science* **1994**, *264*, 819–822.
(14) Smith, D. E.; Chu, S. *Science* **1998**, *281*, 1335–1340.
(15) Teixeira, R. E.; Dambal, A. K.; Richter, D. H.; Shaqfeh, E. S. G.; Chu, S. *Macromolecules* **2007**, *40*, 2461–2476.
(16) Betzig, E.; Trautman, J. K. *Science* **1992**, *257*, 189–195.
(17) Ohtsu, M. *Near-field Nano/Atom Optics and Technology*; Springer: Tokyo, 1998.
(18) Ito, S.; Aoki, H. *Adv. Polym. Sci.* **2005**, *182*, 131–169.
(19) Ube, T.; Aoki, H.; Ito, S.; Horinaka, J.; Takigawa, T. *Polymer* **2007**, *48*, 6221–6225.
(20) Yang, J.; Sekine, R.; Aoki, H.; Ito, S. *Macromolecules* **2007**, *40*, 7573–7580.
(21) Aoki, H.; Morita, S.; Sekine, R.; Ito, S. *Polym. J.* **2008**, *40*, 274–280.
(22) Ube, T.; Aoki, H.; Ito, S.; Horinaka, J.; Takigawa, T.; Masuda, T. *Polymer* **2009**, *50*, 3016–3021.
(23) Aoki, H.; Tanaka, S.; Ito, S.; Yamamoto, M. *Macromolecules* **2000**, *33*, 9650–9656.
(24) Grimaud, T.; Matyjaszewski, K. *Macromolecules* **1997**, *30*, 2216–2218.
(25) Masuda, T.; Kitagawa, K.; Onogi, S. *Polym. J.* **1970**, *1*, 418–424.
(26) Ferry, J. D. *Viscoelastic Properties of Polymers*, 3rd ed.; Wiley: New York, 1980.
(27) Kahar, N.; Duckett, R. A.; Ward, I. M. *Polymer* **1978**, *19*, 136–144.
(28) Marrucci, G.; de Cindio, B. *Rheol. Acta* **1980**, *19*, 68–75.
(29) Rudnick, J.; Gaspari, G. *Science* **1987**, *237*, 384–389.
(30) Viovy, J. L.; Monnerie, L.; Tassin, J. F. *J. Polym. Sci., Polym. Phys. Ed.* **1983**, *21*, 2427–2444.
(31) Fuchs, K.; Friedrich, C.; Weese, J. *Macromolecules* **1996**, *29*, 5893–5901.
(32) Brown, H. R.; Russell, T. P. *Macromolecules* **1996**, *29*, 798–800.